Journal of Applied Fluid Mechanics, Vol. 9, No. 6, pp. 2917-2931, 2016.
Available online at www.jafmonline.net, ISSN 1735-3572, EISSN 1735-3645.

Comparison of Five Two-Equation Turbulence Models for Calculation of Flow in 90° Curved Rectangular Ducts

K. Ma and H. Lai†

School of Mechanical and Power Engineering, East China University of Science and Technology, Shanghai, 200237, P. R. China

†*Corresponding Author Email: hlai@ecust.edu.cn*

(Received September 6, 2015; accepted March 19, 2016)

ABSTRACT

This paper presents a comparative study of five most widely used two-equation turbulence models in predicting the developing flows in two 90° curved rectangular ducts. These include the standard k-ε model, the shear stress transport k-ω model, and three low-Reynolds number k-ε models by Jones and Launder, Launder and Sharma, and Nagano and Hishida, respectively. The computational time for convergent solutions, streamwise and secondary velocities, pressure distributions as well as the Reynolds-averaged turbulence quantities resolved by these models are compared and validated against available experimental data. The purpose of this paper are to provide a detailed comparative verification for applying the five most widely used two-equation turbulence models to predicting curved rectangular duct flows, which are a kind of proto type flows in fluids engineering, and to provide a reference for the selection of turbulence models in predicting such flows in industrial applications.

Keywords: Curved duct flows; RANS (Reynolds-averaged Navier-Stokes); Validation; Predicting capability.

1. INTRODUCTION

Turbulence in a 90° curved duct is a proto type flow in fluid dynamics and fluids engineering. This kind of flows occurs widely in engineering devices such as the cooling coils of heat exchangers and the flow passages in turbo-machinery. The streamline curvature brings great influences on the redistribution of the flow-field. A well known phenomenon is that the turbulence intensity is suppressed by the convex curvature but amplified by the concave curvature (Bradshaw 1973). As the results of the curvature and the pressure gradient, secondary motions, flow energy losses and enhanced heat transfer occur in curved ducts. These phenomena are very different from the flows in straight ducts, and are often decisive to the general performance of the engineering devices.

Because of the academic and practical importance of the curved flows, researchers have devoted huge amount of efforts to study the problem, and a great number of theoretical and experimental investigations have been carried out. Benchmark experimental data of curved duct flows can be found in Humphrey *et al*. (1981), Taylor *et al*. (1982), Kim and Patel (1994), Suzuki and Kasagi (2000), Sudo *et al*. (2001), to name a few. Simple and concise reviews of these experimental studies have been presented by Suzuki and Kasagi (2000) and Sudo *et al*. (2001). Seeing in general, valuable experiments on the three-dimensional velocity components, pressure, heat transfer and turbulent intensity have been made available for the curved ducts of either circular or rectangular sections, with some typical radial ratio values, R_c / d (where R_c is mean curvature radius of the bend and d is the hydraulic diameter of the duct), and in a sensible Reynolds number range widely seen in engineering. These experimental investigations have not only contributed to the understanding of the development of turbulent flow in curved ducts, but also provided detailed observations of secondary motions and turbulence fluctuations in a form suitable for validation of numerical solution techniques and evaluation of turbulence models.

Accurate prediction of the development of the turbulence in the curved ducts is still a challenging task for nowadays computational fluid dynamics (CFD) because of the numerical method. Restricted by the computational resource, early numerical calculations of turbulent flow in curved ducts solved the parabolic or partially parabolic RANS equations (Iacovides *et al*. 1987), which assumed that the flow was not returning even locally in the duct and the diffusion in the streamwise direction was negligible. Apparently, these assumptions may

be conflicted in strongly curved duct flows. On the other hand, low resolution discretization schemes such as the first-order "hybrid" scheme (Rhie 1985) or the "two-point backward difference" (Govindan *et al*. 1991) were widely used in those calculations of turbulent flows in curved ducts. As well known to nowaday's CFD study, these simplifications on the governing equations and the low order discretization schemes are harmful to the resolution of numerical results.

The second difficulty in predicting the curved-duct turbulent flow is the selection of turbulence model. In order to model the effects of curvature on the turbulence field, two-dimensional flow cases were studied by Wilcox and Chambers (1977) and Leschziner and Rodi (1981), and the coefficients of the turbulence model were modified by including the radius of curvature of the streamlines. These modeling methods are basically not applicable to complex three-dimensional flows because of the difficulties in numerically reconstructing the streamlines and defining the curvature. For curved duct turbulent flows, which are naturally three-dimensional, simple eddy viscosity models (EVM) were widely employed by researchers in the early studies of predicting the flow behavior and to reproduce the effects of curvature. Kreskovsky *et al*. (1981) calculated the 90° bend turbulent flow of Taylor *et al*. (1982) using a mean-field closure (one- equation) model. Although a relatively coarse mesh (30 points in radius and 20 points in half-span) was used, satisfactory agreement with the experimental data was still achieved over the first 30° of the bend. Calculation of the same flow was performed by Govindan *et al*. (1991), using a mixing length (zero-equation) model and a finer mesh which has 49×49 nodes in the cross section. Comparisons of streamwise velocity contours were shown, and impressively, very well agreements between the calculation and experimental data were obtained for all cross sections from the upstream to the downstream of the ducts. But unfortunately, no further results were shown by Kreskovsky *et al*. (1981) and Govindan *et al*. (1991). Especially, the wall pressure, the turbulence intensities such as the fluctuating of velocity components and their cross correlations, which had been made available in Taylor *et al*.'s measurements, were not calculated and compared.

In the family of RANS models for turbulence closure, two-equation eddy-viscosity models are widely employed in numerical analysis of curved duct flows. The k-ε type models are the most popular in the two-equation models. Humphrey *et al*. (1981) and Chang *et al*. (1983) employed the standard k-ε model (SKE) combined with the logarithm wall function. Their computational grids were relatively coarse. For example, in Humphrey *et al*.'s calculation of the 90° bend turbulent flow of Taylor *et al*., the mesh had only 11 nodes in half of the span and 14 points in the radial direction in the cross section of the duct. In order to improve the prediction, Iacovides *et al*. (1987) used the SKE in combination with a mixing-length hypothesis wall treatment. Their calculation used a 25×47 mesh to cover the half cross section of the duct between the symmetry plane and the end wall; such a mesh is much finer than that in Humphrey *et al*.'s (1981) study. Meanwhile, the non-diffusive QUICK scheme which was strongly recommended by Chang *et al*. (1983) was applied to the discretization. The calculated streamwise and secondary velocities were presented, and good agreements with experimental data were achieved. Based on these studies, Iacovides *et al*. (1990) employed an algebraic second-moment (ASM) model to compute the U-bend flow. The ASM model obtains the Reynolds stresses from an algebraic statement of their transports, it is still belonging to the family of two-equation models.

The high Reynolds number version of k-ε model cannot be applied in the immediate vicinity of the wall, so it has to be implemented with the so-called logarithm wall function which may loss the universality for complex flows. Low Reynolds number k-ε models (also mentioned as near-wall k-ε models by researchers), however, directly model the turbulent viscosity by introducing a local turbulence Reynolds number and wall-damping functions. These models allow integration of the transport equations for both k and ε to the wall, at a cost of more intensive computational task. Application of Launder and Sharma's low-Re-number k-ε model (1974) to 90° curved rectangular ducts has been attempted by Raisee *et al*. (2006). In order to further improve the predicted results, a cubic nonlinear low-Re-number k-ε model (Craft *et al*. 1996) was included in their calculations. The results showed that both linear and non-linear low-Re-number k-ε models produced satisfactory predictions of the mean flow field, while the non-linear model returned even better predictions of the turbulence intensity quantities. Although no-surprisingly near-wall second moment closures (Suga 2003) showed superiority in the results of Reynolds stress, the question of whether it worth to proceed with a complex turbulence model was not answered yet by researchers. Meanwhile, for non-linear models, numerical instability induced by high-order derivatives has to be suppressed so as to guarantee the convergence of calculation (Speziale and Ngo 1988). The side effect of such suppression or filtering on the resolution of numerical results is not known yet. Indeed, despite the well-known deficiencies primarily related to the isotropic behavior, linear two-equation models are still the first choice for industrial purpose of a quick and stable prediction of complex flow fields.

Another important and attractive two-equation eddy-viscosity model is the shear stress transport k-ω model (SST). The model can also be integrated to the wall and does not require a wall function. The SST model is originally developed for prediction of aeronautics flows with strong adverse pressure gradients and separation (Menter 1993, 1994), but has since made its way into most industrial, commercial and research codes. The SST model is also criticized for being not capable of capturing the effects of streamline curvature and system rotation, so modifying the model so as to make it sensible to

rotation and curvature has been attempted by researchers in these years (Shur *et al*. 2000; Dhakal and Walters 2011). By so far, application of the original SST model to calculate flows with streamline curvature is mainly for two-dimensional (2D) cases such as the flow in U-turn (Dhakal and Walters 2011). Shur *et al*. (2000) compared the calculations of Kim and Patel's 90° rectangular bend using the SST and three other models, the results of skin-friction distribution were presented and compared with experimental data. The study supported that a scalar eddy-viscosity model was able to treat the rotation and curvature properly if the sensitization method by Spalart and Shur (1997) was applied. However, no further calculated result about the curved duct was presented by Shur *et al*. (2000). Therefore, the validation and comparison by Shur *et al*. were too incomplete to provide a reference for selection of turbulence models in calculating curved duct flows.

Based on the status quo of the research on curved duct flows mentioned in above, the present paper presents a comparative study of five most widely used two-equation turbulence models in predicting the developing flows in two 90° curved rectangular ducts. The models are the standard *k*-*ε* model (SKE), the shear stress transport *k*-*ω* model (SST), and three low-Reynolds number *k*-*ε* models by Jones and Launder (1972; JL), Launder and Sharma (1974; LS) and Nagano and Hishida (1987; NH). Two 90° curved ducts which have benchmark experimental data measured by Taylor *et al*. (1982) and Kim and Patel (1994), respectively, are selected as testing cases for consideration the effects of geometrical aspect ratio on the flow fields. In a curved duct of large aspect ratio, the flow is nominally two-dimensional, while the flow in a square duct is fully three-dimensional. The major difference between these two cases is the scale and the influenced region of the secondary motions. The main objective of this paper is to compare the performances of these five simple two-equation eddy-viscosity models in predicting the curved duct flows. The computational time for convergent solutions, the streamwise and secondary velocities, the pressure distributions as well as the Reynolds-averaged turbulence quantities resolved by these models will be compared and discussed.

2. GOVERNING EQUATIONS AND NUMERICAL METHOD

Consider the Reynolds-averaged Navier-Stokes equations for three-dimensional, incompressible and steady flows, the conservation laws of mass and momentum are written as,

$$\frac{\partial \overline{u}_j}{\partial x_j} = 0 \tag{1}$$

$$\frac{\partial \overline{u}_j \overline{u}_i}{\partial x_j} = -\frac{1}{\rho}\frac{\partial p}{\partial x_i} + \frac{\partial}{\partial x_j}\left(\nu \frac{\partial \overline{u_i}}{\partial x_j} - \overline{u_i' u_j'}\right) \tag{2}$$

where p is the pressure, ν is the kinematic viscosity, $\overline{u_i}$ and u_i' denote the mean and fluctuating velocities, respectively. $-\overline{u_i' u_j'}$ is the Reynolds stress which may be calculated using the Boussinesq eddy-viscosity-approximation:

$$-\overline{u_i' u_j'} = -\frac{2}{3}\delta_{ij}k + \nu_t\left(\frac{\partial \overline{u_j}}{\partial x_i} + \frac{\partial \overline{u_i}}{\partial x_j}\right) \tag{3}$$

where the turbulence kinetic energy $k = \frac{1}{2}\left(u'^2 + v'^2 + w'^2\right)$, ν_t is the eddy viscosity.

For the closure of the above equations, a turbulence model must be introduced. In the present work, five turbulence models are used; they are the SKE, SST, JL, LS and NH. These models are all among the most widely used and are based on the eddy-viscosity assumption. The details of the SST model can be found in Menter's study (1994). In the four *k*-*ε* type models (*ε* is the dissipation rate of *k*), the transport equations for *k* and *ε*, respectively, are as follows:

$$\frac{\partial(\overline{u}_j k)}{\partial x_j} = \frac{\partial}{\partial x_j}\left[\left(\nu + \frac{\nu_t}{\sigma_k}\right)\frac{\partial k}{\partial x_j}\right] + \nu_t\left(\frac{\partial \overline{u_i}}{\partial x_j} + \frac{\partial \overline{u_j}}{\partial x_i}\right)\frac{\partial \overline{u_i}}{\partial x_j} - (\varepsilon + D) \tag{4}$$

$$\frac{\partial(\overline{u_j}\varepsilon)}{\partial x_j} = \frac{\partial}{\partial x_j}\left[\left(\nu + \frac{\nu_t}{\sigma_\varepsilon}\right)\frac{\partial \varepsilon}{\partial x_j}\right] + C_1 f_1 \frac{\varepsilon}{k}\nu_t \overline{u_i' u_j'}\frac{\partial \overline{u_i}}{\partial x_j} - C_2 f_2 \frac{\varepsilon^2}{k} + E \tag{5}$$

where C_μ, C_1, C_2, σ_k and σ_ε are the model constants, the eddy viscosity ν_t is then calculated by:

$$\nu_t = C_\mu f_\mu \frac{k^2}{\varepsilon} \tag{6}$$

f_1, f_2 and f_μ are damping functions while D and E are additional terms for consideration of the wall effects. The formula and constants for models can be found in relevant literature.

Eqs. (1), (2), (4) and (5) can be written in a general form as follows:

$$\nabla \cdot \left(\vec{u}\phi - \Gamma_\phi \nabla \phi\right) = S_\phi \tag{7}$$

where $\vec{u}$ is the velocity vector, Γ_ϕ is the diffusion coefficient of ϕ, and S_ϕ is the source term. ϕ represents the dependent variable (which is 1, $\overline{u_i}$, k or ε) according to transport equations. For the momentum equation, the pressure gradient is included in the S_ϕ.

Integrating Eq. (7) over the control volume surrounding the node P and shown in Fig. 1, we have:

$$\sum_f C_f - \sum_f D_f = \left(S_\phi V\right)_P \tag{8}$$

where the summation is applied to all the facets of

the control volume V, i.e., $f = n$, s, e, w, b, and t (see Fig. 1). C_f and D_f are the transport fluxes through the face f due to convection and diffusion, respectively:

$$C_f = \left(\vec{u}\phi\right)_f \cdot \vec{A}_f = F_f \phi_f \tag{9}$$

$$D_f = \Gamma_f \left(\nabla\phi\right)_f \cdot \vec{A}_f \tag{10}$$

where $\vec{A}_f$ is the area of f.

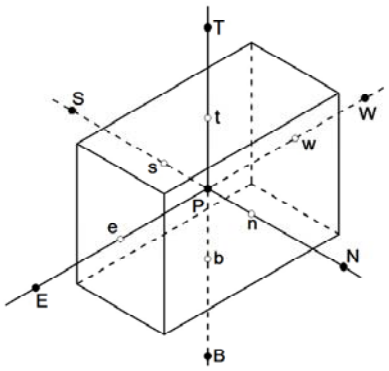

Fig. 1. Control volume surrounding node P.

The diffusive terms D_f is calculated by the central difference scheme. For considerations of both high order accuracy of numerical results and stability of calculation, the convection term is discretised by using the third-order SMART scheme (Gaskell and Lau 1988) and is implemented with a so-called "deferred correction" method. Denote the cell-face values of ϕ_f calculated by the first-order upwind (UPW) scheme and a high-order scheme with ϕ_f^{UPW} and ϕ_f^H, respectively, the convection term becomes:

$$C_f = F_f \phi_f^H = F_f \phi_f^{UPW} + F_f \left(\phi_f^H - \phi_f^{UPW}\right) \tag{11}$$

With these treatments, Eq. (7) is discretised into the final form as follows:

$$a_{\mathrm{P}} \phi_{\mathrm{P}} = \sum a_{\mathrm{N}_i} \phi_{\mathrm{N}_i} + b \tag{12}$$

where the subscript N_i denotes the neighbor nodes N, S, E, W, B and T, shown in Fig. 1. The coefficients a_{P}, a_{N_i} and b in discretization Eq. (12) and details about solution procedure are given by Lai *et al*. (2011). The solution of the governing equations is based on the SIMPLE algorithm (Patankar 1980). The calculations in this paper are carried out using an in-house code which uses a finite-volume grid arrangement in non-orthogonal system. The code is written using the FORTRAN computer language, and is parallelized according to the Open MP protocol for running on a small computer workstation which has 20 processing elements.

For the simplicity of comparing the computational time in the present study, all the algebraic equations in the form of Eq. (12) are solved using the tri-diagonal matrix method (TDMA) and applying an alternating direction implicit (ADI) strategy in the three coordinate directions. During a solution step, the coefficients in Eq. (12) are kept fixed for three to five iteration steps using the TDMA and ADI method, then the temperate results of ϕ_{P} are employed to update the coefficients of the discrete Eq. (12) so as to carry out a new solution step. Meanwhile, under relaxation is applied. The relaxation factors for pressure, velocity and turbulence quantities are set to be the same for calculations of using all the five turbulence models, namely, $\alpha_{p'} = 0.7$, $\alpha_{\vec{u}} = 0.3$, and $\alpha_{turb.} = 0.3$, respectively. Further, for checking the convergence of calculations, denote the flow rate of a curved duct by Q, the calculated flow rate at a cross-section as Q_1, convergence of calculation is judged by satisfying the criteria:

$$\begin{cases} E_1 = \dfrac{\max\left(\left|Q - Q_1\right|\right)}{Q} < 10^{-3}, \\ E_2 = \dfrac{\sum \left|m_P\right|}{Q} < 10^{-4} \\ E_3 = \dfrac{\max\left(\left|m_P\right|\right)}{Q} < 10^{-6} \end{cases} \tag{13}$$

where m_p is the unbalanced mass source of the pressure correction equation. The values of m_p for all grid nodes should be zero when the continuity equation is satisfied (Patankar 1980).

As pointed out by Shur *et al*. (2000), difficulties for imposing the inlet boundary conditions are encountered for computing these flows, due to the lack of experimental data on the mean and turbulent flow quantities in the near-wall region of the reference section of the duct. In this paper, the inlet boundary conditions are imposed by set the inflow velocity U equal to the bulk velocity U_{c}, the velocity components in the cross-section and normal to the bulk flow. Secondary velocities V and W at the inlet boundary are set to be zero. The inflow conditions for k and ε are imposed according to fully developed pipe flow, *i.e*., $k_{\mathrm{in}} = (0.5\sim1.5)\% \times U_{\mathrm{c}}^2/2$, and $\varepsilon_{\mathrm{in}} = C_\mu k_{\mathrm{in}}^{3/2}/(0.03L)$, where L is the characteristic length of the flow. At the downstream boundary, zero gradient conditions are imposed for all variables except pressure. The no-slip condition is assigned for the velocity on solid walls, while wall conditions applied for k and ε are not summarized here for limited space.

3. TESTING CASES AND RESULTS

For convenience of description, depict the two 90° curved ducts experimentally studied by Taylor *et al*. (1982) and Kim and Patel (1994), respectively, as Case A and Case B. Fig. 2(a) shows the geometry of Case A. The bound of square cross-section is d = 40 mm, and the mean bend radius is 92 mm, which result in a radius ratio of 2.3. The upstream and downstream tangent lengths are 0.3 m and 0.8 m, respectively. The bulk velocity U_{c} = 1 m/s,

corresponding to the Reynolds number, *Re*, of 40000. Fig. 2(b) is the configuration of Case B. The curved duct is of rectangular cross-section with an aspect ratio of 6 and the duct width H = 0.203 m. The lengths of the duct before and after the curved section are 8*H* and 26*H* respectively. The bulk velocity is U_c = 16 m/s, and then *Re* = 224000. X_H is the coordinate in upstream (X_H takes negative value) and downstream (X_H is positive) tangents of the bend, normalized by the hydraulic diameter *d*. In Case A, r^* is the normalized radial coordinate, $r^*=(r-r_o)/(r_i-r_o)$; z^* is the normalized spanwise coordinate, $z^*=z/(0.5d)$, so $z^*=0$ is the symmetry plane of curved duct while $z^*=1$ is the side wall. In Case B, Y is normalized radial coordinate, so $Y=0$ and 1 are the outer and inner walls, respectively. And z^* is the normalized by the duct width H in this case, $z^*=z/H$.

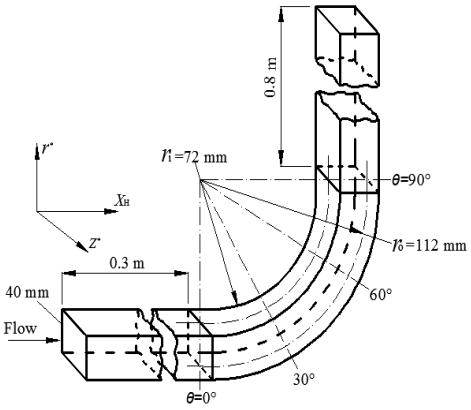

(a) Case A

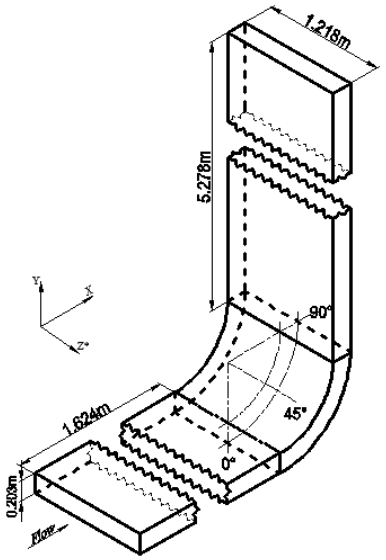

(b) Case B

Fig. 2. Geometry of two curved ducts.

3.1 Grid-Dependency Check

Grid-dependency check is performed before comparing the results of turbulence models. Three grids are tested for each case, respectively, and the number of nodes is summarized in Table 1. All the tested grids are stretched in cross-sections so as to resolve the flow fields near the walls.

Figure. 3 is the example of checking the grids for Case A. The streamwise velocity profiles calculated using the LS at θ=30° are shown. At this plane, the core fluid still remains at the inner wall. It can be seen that grid-refining from Mesh A1 to A2 has produced a noticeable difference in the velocity profiles. However, when the grids are further refined, from Mesh A2 to A3, the plotting differences between the two numerical results are negligible. Therefore, Mesh A2 is believed to be fine enough to produce a grid-independent numerical solution. Similarly, Mesh B2 is selected for Case B.

Table 1 Mesh for grid-dependency check

	Number of grid points		
Case	Radial	Spanwise	Streamwise
Mesh A1	30	30	102
Mesh A2	56	56	102
Mesh A3	76	76	102
Mesh B1	80	90	172
Mesh B2	116	114	172
Mesh B3	136	130	172

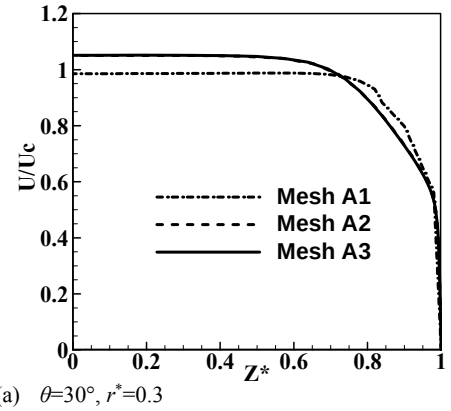

(a) θ=30°, r^*=0.3

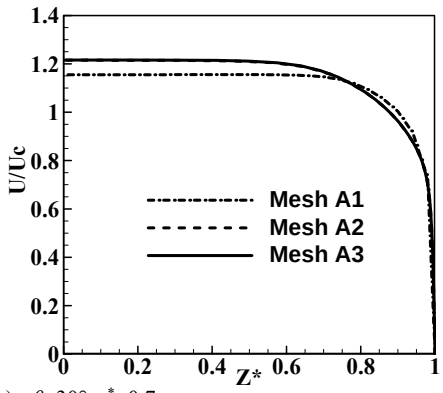

(b) θ=30°, r^*=0.7

Fig. 3. Streamwise velocity profiles calculated by three meshes in Case A.

The five models have been carefully tested for the grid-dependency, and the results show that Mesh A2 and Mesh B2, for Case A and Case B respectively, are fine enough for all the five models. So for the simplicity and clarity of comparison between turbulence models, the numerical results and analyses in the followed sections are based on using these selected meshes, i.e., Mesh A2 and Mesh B2 for Case A and Case B, respectively.

3.2 Computational Time

The needed iteration steps for convergence, tolerance and computational time for all the tested models are summarized and presented in Table 2. In Case A, the needed iteration steps for solution convergence using SST , JL, LS and NH models are less than SKE model, however, the computational time for SKE is less than other models, because of the lighter computational task for the SKE in a solution step. In Case B, low-Reynolds-number k-ε models and SST model have similar iteration steps for convergence. On the other hand, the number of needed solution steps for SKE is slightly more than other models. Identical to the situation in Case A, the computational efficiency of the SKE is the highest among the five turbulence models.

Table 2 Computational efficiency of five models

Models	Iter. steps	E_3	Time
SKE	10000	1.0E-8	2.5h
SST	2500	1.0E-8	2.6h
JL	2500	1.0E-8	2.6h
LS	2500	1.0E-8	2.6h
NH	2500	1.0E-8	2.6h

(a) Case A

Models	Iter. steps	E_3	Time
SKE	4800	1.0E-8	8h
SST	4200	1.0E-8	8.2h
JL	4200	1.0E-8	8.2h
LS	4200	1.0E-8	8.2h
NH	4200	1.0E-8	8.2h

(b) Case B

3.3 Basic Features of the Two Cases

Before comparing the results predicted by different models, the basic features of the flow fields calculated by using the LS in the two cases are compared and presented in Fig. 4 to 6.

Figure. 4 compares the streamwise velocity profiles in the symmetric planes of the ducts, at θ=45° and 90°. At θ=45°, the maximum velocity of two ducts occurs both near the inner wall of the bends (where $r=r_i$ or Y=1, see Fig. 2). The radial gradients of the velocity near the outer side of the bends (where $r=r_o$ or Y=0, also please see Fig. 2) are less steep than near the inner wall. At the outlet of the bends, θ=90°, the velocity profile for Case B remains similar to that at θ=45°, but its value becomes more uniform along the radial direction. For Case A, the peak of streamwise velocity at θ=90° has moved to the duct center, the velocity gradient at the outer wall becomes steeper than at the inner wall. Seeing from velocity profiles in Fig. 4, the flow in Case A is more complex and fully three-dimensional. On the other hand, the flow in Case B has the characteristics of nominally two-dimensional flow.

The pressure distributions along the centerlines of the outer and inner walls are shown in Fig. 5, where the pressure coefficient C_p, is defined as:

$$C_p = \left(p - p_{ref}\right) \Big/ \left(0.5\rho U_c^2\right) \tag{14}$$

It can be seen that the radial pressure gradient (the difference of pressure coefficient between the outer and inner walls at every streamwise location) in Case A is steeper than that in Case B. On the inner wall, Case A's minimum pressure coefficient occurs at θ=30°, indicating that the favorable pressure gradient turns into the reversed at the location. Such trough of the C_p also means the flow is changed from accelerating to decelerating. But in case B, the pressure coefficient decreases mildly along the walls, except in the regions near the inlet and outlet of the bend, means the flow velocity in Case B is remained nearly uniform along the streamwise of bend.

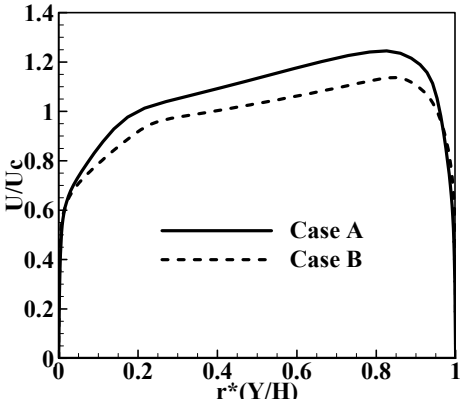

(a) θ=45°

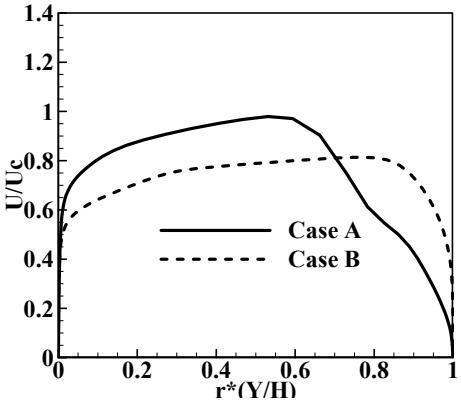

(b) θ=90°

Fig. 4. Streamwise velocity profiles along symmetrical centerline calculated by LS model.

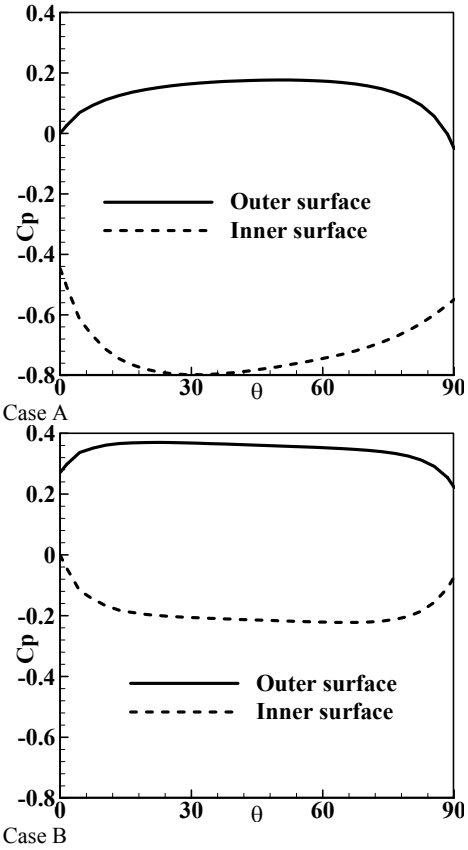

Fig. 5. Pressure coefficients along the centerline of the outer and inner walls, calculated by LS.

The most noticeable difference between two cases is the area influenced by secondary motion shown in Fig. 6 (cross-section at θ=90°, right side of the cross section is the inner surface of the bend; In Case B, only one third of the cross-section is shown for the secondary velocity vectors). Compared with that in the Case A, the secondary motion in the Case B is weaker and is confined to the corner regions near the sidewalls. Because of the large aspect ratio, the area influenced by the secondary motion is very limited. Therefore, the flow field in Case B shows some nominally two-dimensional characters. In Case A, a pair of counter rotating vortices occupy the area of almost the whole cross section, and the magnitude of the secondary velocity is also larger.

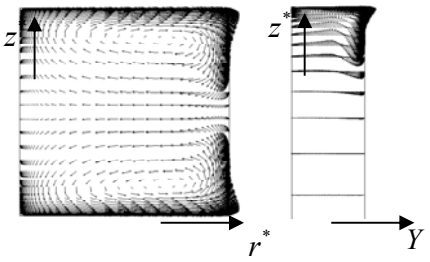

(a) Case A (b) Case B

Fig. 6. Secondary flow vectors.

3.4 Validation and Comparison

Case A

The streamwise velocity in cross-sections and calculated by using the five turbulence models are compared with the experimental data and are shown in Fig. 7. The results of JL, LS and NH models almost duplicate with each other. It can be seen that the flow is still developing in the upstream of the bend (Fig. 7(a), X_H= -0.25), and all the five models give a similar profile in the core region. Within the curved section, at θ=30°, the five models perform similarly except in close to the outer wall, i.e., at r^*=0.1 in Fig. 7(b), where none of the five models agree well with the experimental data. At θ=60° (shown in Fig. 7(c)), the differences between the models are mainly found at in close to the inner wall, at r^*=0.9. Due to the secondary motion, the low-momentum fluid particles are accumulated in this region. The NH model has obtained the worst prediction, as compared with the other four models and the experimental data. Such transport and accumulation of low-momentum fluid particles by secondary motion (see Fig. 6) are carried on until the downstream of the curved section, at r^*=0.7 and 0.9 in the cross-section X_H=0.25 (Fig. 7 (d)). The streamwise velocity becomes very low in this region and flow separation is possibly to occur locally, although it is not clearly observed in the present calculation. The SST predicted this trough of streamwise velocity quite well, and so did the low-*Re* k-ε models except the NH. The SKE also predicted the streawise velocity correctly at r^*=0.7, but at r^*=0.9, the predicted velocity by the SKE is quite lower than the measured value.

Figure.8 shows the calculated radial component of the secondary velocity, V. As compared with the experimental data, it can be seen that the four k-ε models return almost the same results in these cross-sections again. In all these cross-sections, the SST performs the best in predicting the secondary motion.

In Fig. 9, the predicted contours of the turbulent kinetic energy at X_H=2.5 are compared with the corresponding measured data. It can be seen that the results of the low-*Re* k-ε models JL and LS are very similar to each other, and their predicted peak-value contour lines, scale of 1.4, are in good agreement with the experiment, either in terms of the location and the scale value. Such peak-value contour line is also predicted well by the SST. However, the low turbulent kinetic energy zones in near the middle of outer wall and in near the inner wall are over predicted by the SST; its predicted values are lower than the measured. On the other hand, the predictions for these low value zones using JL and LS are fairly good and acceptable. The NH model under predicted the peak value of the kinetic energy though the location of the peak is also approximately correct. The SKE over predicted the peak of the kinetic energy; the area enclosed by the peak-value contour line predicted by SKE is far larger than the experimental result of Taylor *et al*. (1982).

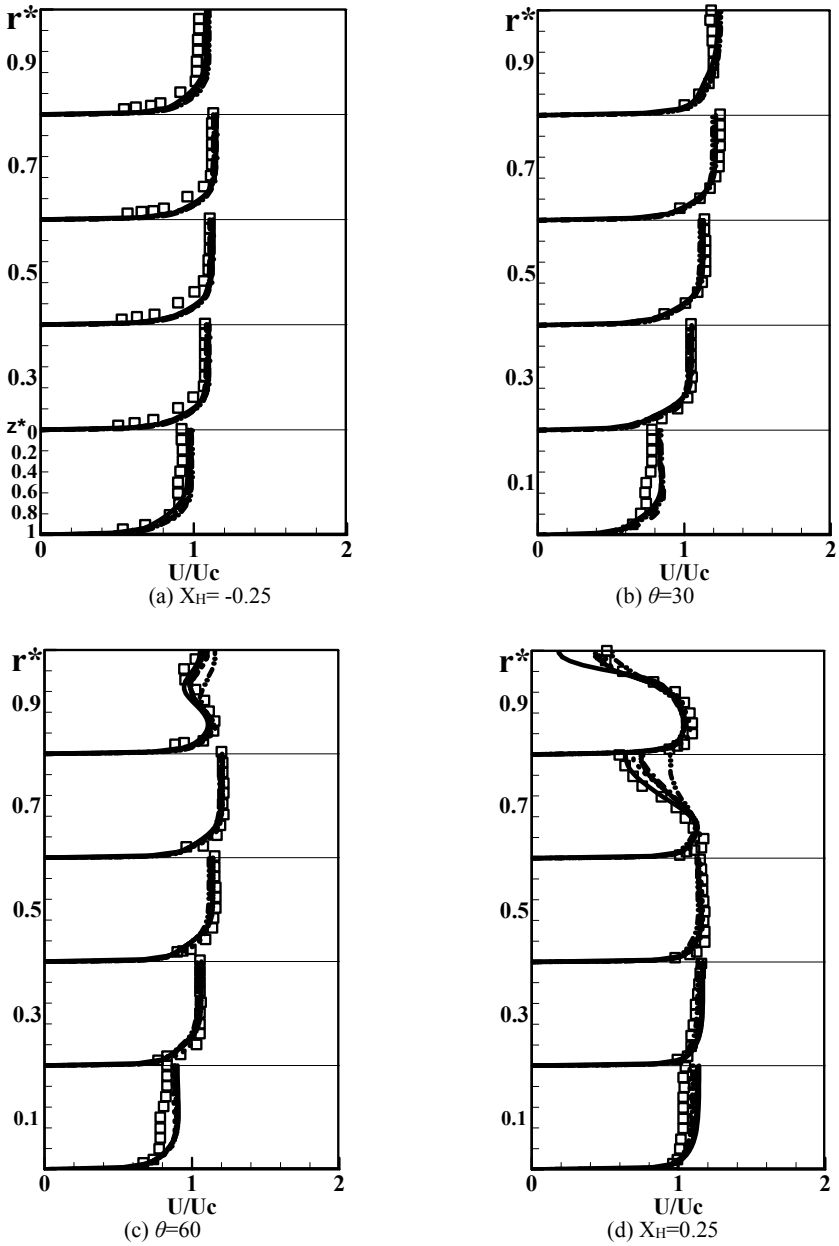

Fig. 7. Predicted streamwise velocity of Case A.
(JL; LS; NH; SST; SKE; □ Taylor *et al*. 1982)

In the literature, the turbulence quantities for the present Case A are seldom presented in evaluating the turbulence models. The predicted contours of the turbulence cross-correlation and fluctuating velocities, namely, $\overline{u'v'}$ and $\tilde{u}'$ in the cross-section X_H=2.5 are shown in Fig. 10 and 11, respectively, and are compared with experimental data. For the cross-correlation $\overline{u'v'}$ shown in Fig. 10, it seems all the results of the five models have basically agreed with the measured distribution, the result of the LS seems the best in amongst of the five models. For the fluctuating intensities $\tilde{u}'$ shown in Fig. 11, the situation is quite similar to the turbulent kinetic energy, shown in Fig. 9. The low-*Re* k-ε models JL and LS return quite similar contours, which are in good agreement with the experiment, either in terms of the location and the scale values. The SST also has predicted the peak values of the intensities well. However, the low value zones in near the middle of outer wall and in near the inner wall predicted by the SST are lower than the measured. The predicted fluctuating intensities by the NH model are fairly acceptable as compared with the experimental data. The value levels of the contour lines predicted by the SKE are generally higher than the experimental results.

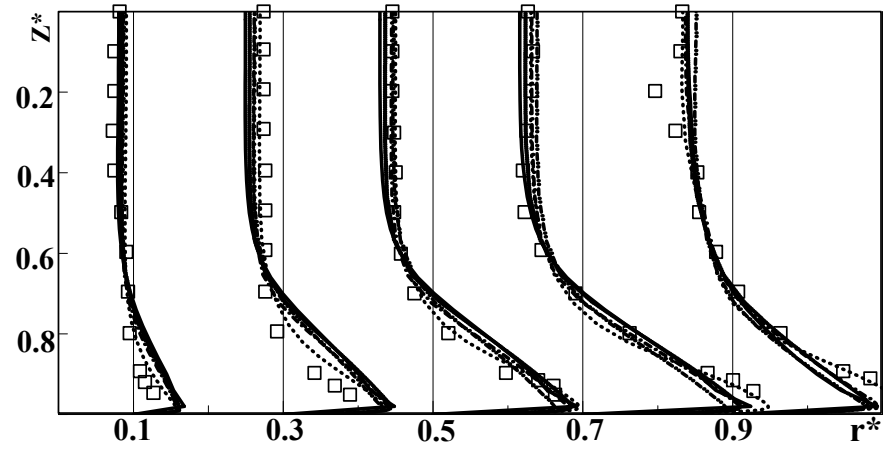

(a) θ=60

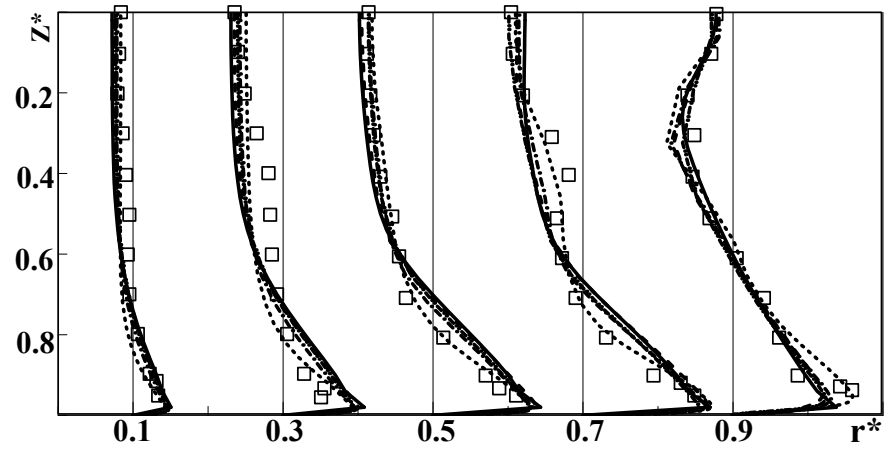

(b) X_H=0.25

Fig. 8. Predicted radial velocity of Case A
(— · — JL; ····· LS; – – – NH; ——— SST; ——— SKE; □ Taylor *et al*. 1982).

Case B

Again, the predictions of both the mean flow velocity and turbulent fluctuating quantities are employed to evaluate the performance of turbulence models in modeling flow characteristics through the curved duct. U_{ref} stands for the free-stream velocity at the reference station X_H=-4.5. It is used to normalize the velocity and the Reynolds-averaged turbulence quantities.

The predicted streamwise velocity profiles at some sections in Case B are shown in Fig. 12. To validate the present calculation, the numerical results by Raisee *et al*. (2006) are included; their calculation also used the LS model. Fig. 12 shows that present results of using the LS model have better agreements with the experimental data (Kim and Patel, 1994) than those by Raisee *et al*. (2006). The presently calculated profiles are more close to the measured results, possibly due to the high resolution numerical methods adopted here. There is very little notable difference between turbulence models in the predicted streamwise velocities, except at downstream of the bend and close to the side wall, as shown in Fig. 12 (d). At such location, none of the selected models makes a good agreement with the measured data. The early analysis shows that the secondary motion is strongest at about X_H=0.5 and z^*=2.5. The secondary vortex introduces a point of inflection in the velocity profile. According to the measured data, the maximum of the streamwise velocity appears at about Y/H=0.7. The result of the SST model seems agreed slightly better than the other four models with the experimental data.

In Fig. 13, the predicted and measured turbulent kinetic energy profiles are compared. At the curved section θ=45° (Fig. 13(a) and (b)), it is seen that all selected models under-predict the peak turbulence kinetic energy near the outer wall (Y=0, i.e., the outer wall of the bend). In downstream of the curved section, at X_H=0.5 and z^*=2.5 (Fig. 13(c) and (d)), the discrepancies between predictions and experimental data are quite clear in near the outer wall of the bend. Only the tendency of variation is

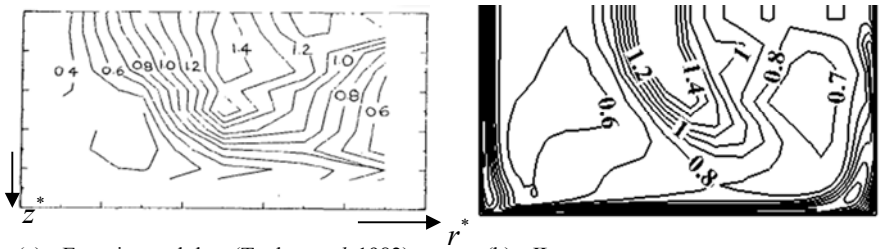

(a) Experimental data (Taylor *et al*. 1982) (b) JL

(c) LS (d) NH

(e) SST (f) SKE

Fig. 9. Predicted turbulent kinetic energy $k / U_C^2(\times 100)$ contours at X_H=2.5 for Case A.

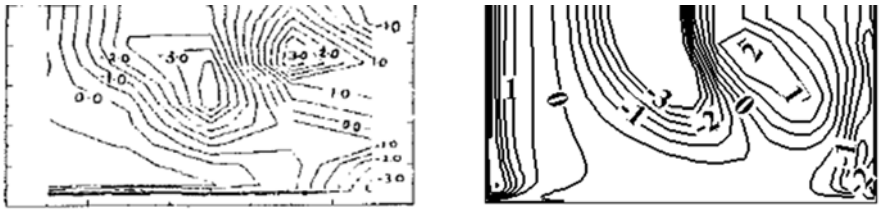

(a) Experimental data (Taylor *et al*. 1982) (b) JL

(c) LS (d) NH

(e) SST (f) SKE

Fig. 10. Predicted contours of $-\overline{u'v'}/U_C^2(\times 1000)$ at X_H=2.5.

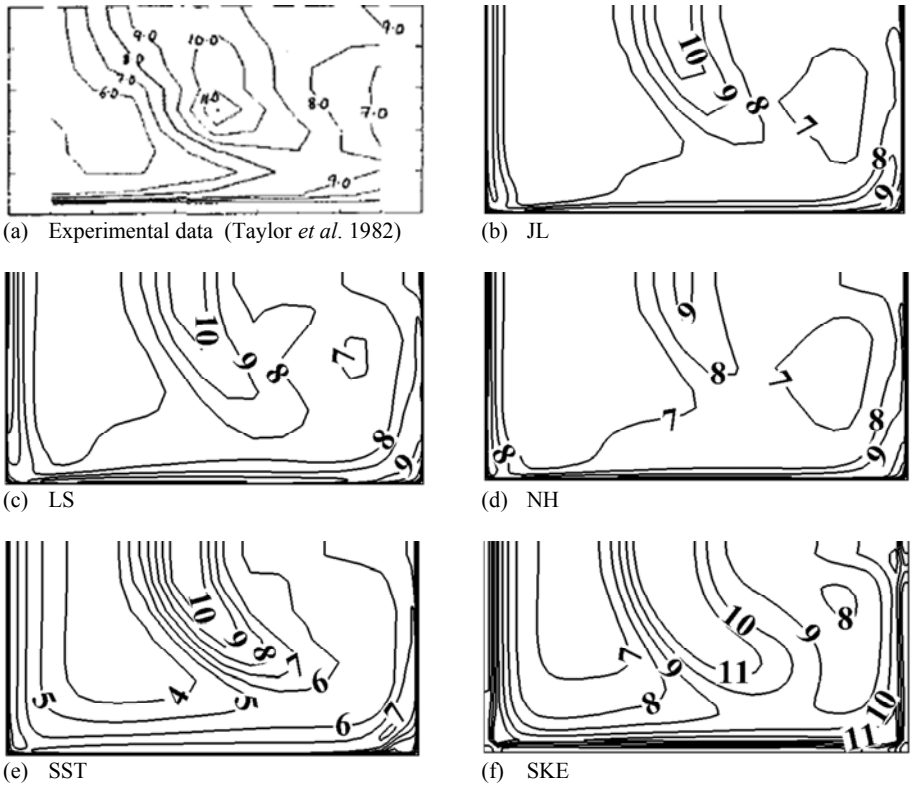

(a) Experimental data (Taylor *et al*. 1982) (b) JL

(c) LS (d) NH

(e) SST (f) SKE

Fig. 11. Predicted contours of $\tilde{u}/U_C(\times 100)$ at X_H=2.5.

approximately agree with the experiment. In the five models, the LS model produces a prediction relatively better than other models. Again, Raisee *et al*'s (2006) calculated results using the LS model are also included for comparison. Although the turbulence model for the two calculations is the same, the present calculation is more close to the measurement, possibly because of our high resolution code.

The comparisons for turbulent stresses are shown in Fig. 14 and 15. Similar to turbulent kinetic energy, the results obtained by five models are basically alike in the core region in the upstream of the curved section. The LS model performs better than the other four models. Differences between the five models become noticeable near the outer and inner walls, especially in the curved section, at θ=45° for example. In downstream of the bend, the agreement between numerical and experimental results is generally poor, though the LS model results a slightly better prediction.

4. CONCLUSION

Even in nowadays, two-equation RANS models are still important choices for industrial purpose of predicting complex flow fields. In this paper, five widely used two-equation turbulence models are compared in predicting the developing flows in two 90° curved ducts. The computational efficiency, the predicted streamwise and secondary velocities, the pressure distributions as well as the Reynolds-averaged turbulence quantities resolved by these models are compared and validated against available experimental data. The main conclusions are summarized as follows:

a. The numerical results indicate that the computation efficiency of the SKE is the highest among the five turbulence models for both the fully three-dimensional and the nominally two-dimensional 90°-curved-duct flows. However, the predicting capability of the turbulence quantities by the SKE is generally poor.

b. The velocity profiles predicted by the SST model show better agreements with experimental data than the other four models in the fully three-dimensional case. The model also obtains a slightly better prediction of the velocity profile in the secondary vortex center. But unfortunately, the predicting capability of the turbulence quantities by the SST is also relatively poor.

c. In the two tested cases, the predicted results by the JL and LS models are very similar. As compared with available data, the two low-Re number models obtained better agreements than the SKE and the SST models. The LS model returns better predictions for the Reynolds stresses and the turbulent kinetic energy. Validations by experimental data show that the capability of predicting turbulence quantities is indeed a

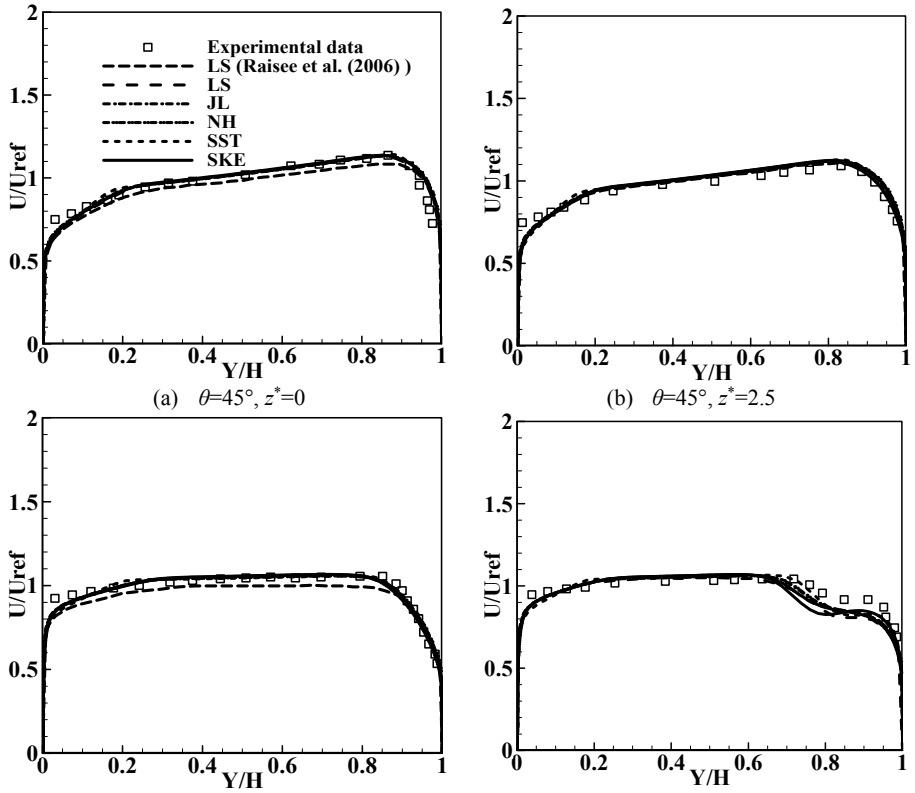

(a) θ=45°, z^*=0 (b) θ=45°, z^*=2.5

(c) X_H=0.5, z^*=0 (d) X_H=0.5, z^*=2.5

Fig. 12. Predicted streamwise velocity profiles.

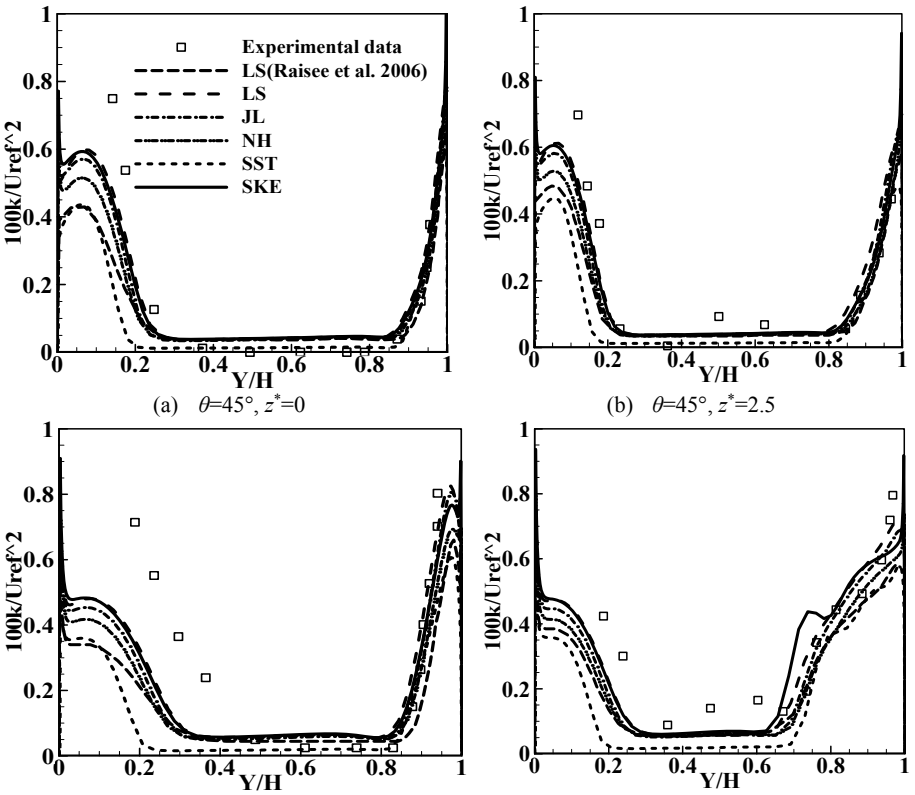

(a) θ=45°, z^*=0 (b) θ=45°, z^*=2.5

(c) X_H=0.5, z^*=0 (d) X_H=0.5, z^*=2.5

Fig. 13. Predicted turbulent kinetic energy $k/U_{ref}^2(\times 100)$.

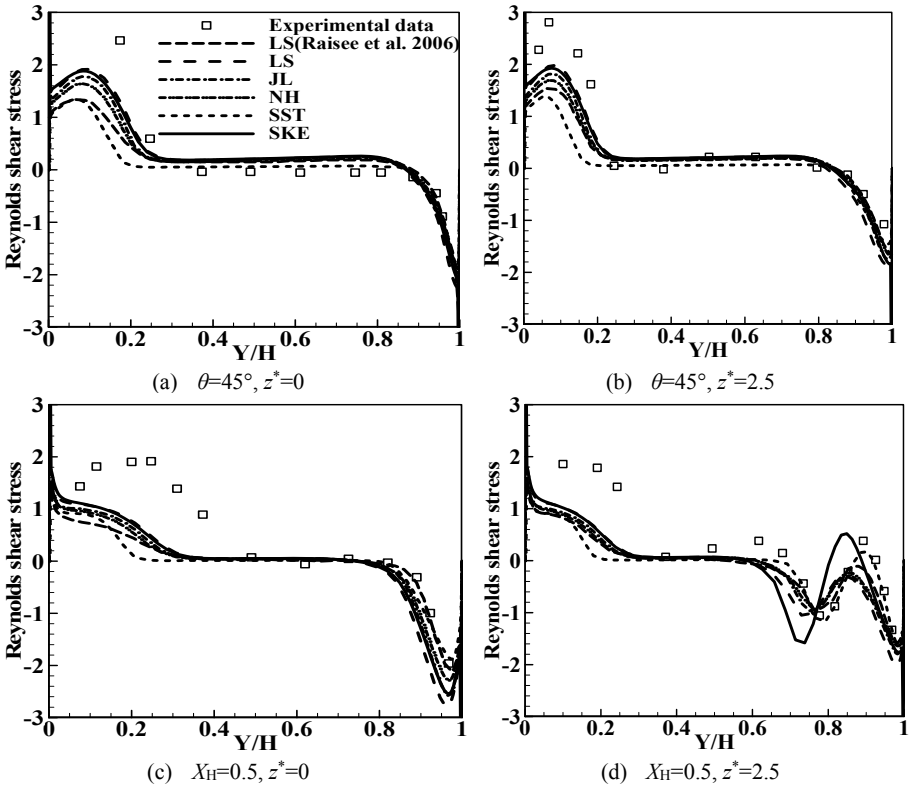

(a) θ=45°, z^*=0 (b) θ=45°, z^*=2.5

(c) X_H=0.5, z^*=0 (d) X_H=0.5, z^*=2.5

Fig. 14. Predicted cross-correlation $-\overline{u'v'}/U_{ref}^2$ (×1000).

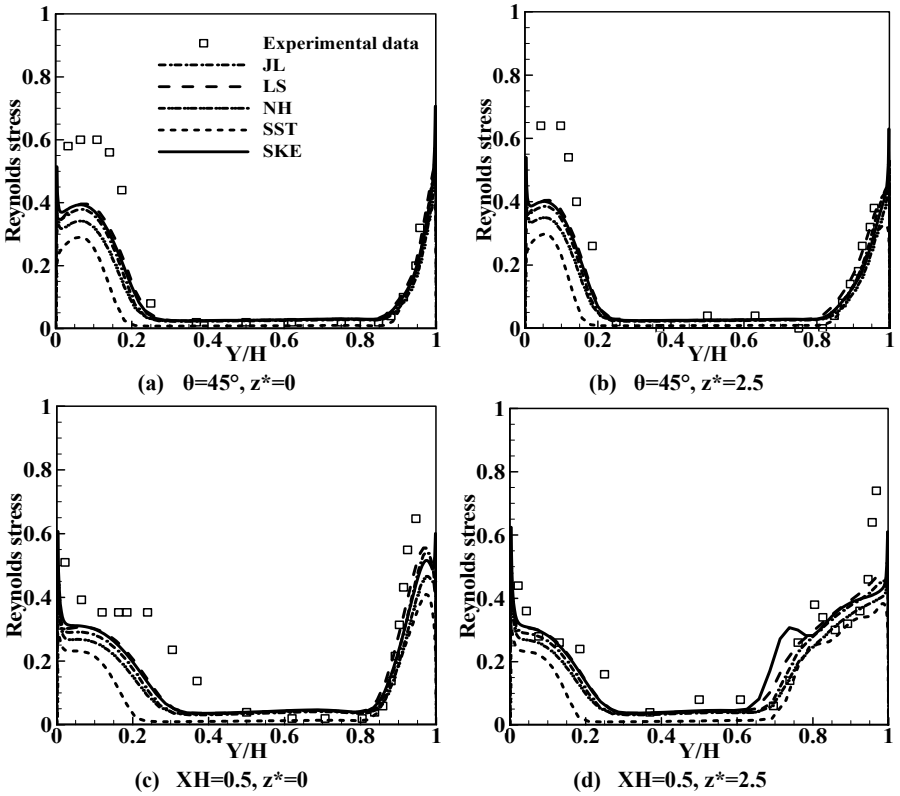

(a) θ=45°, z*=0 (b) θ=45°, z*=2.5

(c) XH=0.5, z*=0 (d) XH=0.5, z*=2.5

Fig. 15. Distributions of Reynolds normal stress $\overline{u'u'}/U_{ref}^2$ (×100).

weakness for the five two-equation models. However, the LS model has still provided relatively more favorable predictions than the other four models in this paper.

ACKNOWLEDGEMENTS

This study is funded by the National Natural Science Foundation of China (NSFC) under grants 51576067 and 51176048.

REFERENCES

Bradshaw, P. (1973). Effects of streamline curvature on turbulent flow. *Advisory group for aerospace research and development*, Paris, France.

Chang, S. M., J. A. C. Humphrey and A. Modavi (1983). Turbulent-flow in a strongly curved U-bend and downstream tangent of square cross-sections. *PhysicoChemical Hydrodynamics* 4(3), 243-269.

Craft, T. J., B. E. Launder and K. Suga (1996). Development and application of a cubic eddy-viscosity model of turbulence. *International Journal of Heat and Fluid Flow* 17(2), 108-115.

Dhakal, T. P. and D. K. Walters (2011). A three-equation variant of the SST k-ω model sensitized to rotation and curvature effects. *Journal of Fluids Engineering* 133(11), 111201.

Gaskell, P. H. and A. K. C. Lau (1988). Curvature compensated convective transport: SMART, A new boundedness□preserving transport algorithm. *International Journal for Numerical Methods in Fluids* 8(6), 617-641.

Govindan, T. R., W. R. Briley and H. McDonald (1991). General three-dimensional viscous primary/secondary flow analysis. *AIAA journal* 29(3), 361-370.

Humphrey, J. A. C., J. H. Whitelaw and G. Yee (1981). Turbulent flow in a square duct with strong curvature. *Journal of Fluid Mechanics* 103, 443-463.

Iacovides, H., B. E. Launder and P. A. Loizou (1987). Numerical computation of turbulent flow through a square-sectioned 90 bend. *International Journal of Heat and Fluid Flow* 8(4), 320-325.

Iacovides, H., B. E. Launder, P. A. Loizou and H. H. Zhao (1990). Turbulentboundary-layer development around a square-sectioned U-bend: measurements and computation. *Journal of Fluids Engineering* 112(4), 409-415.

Jones, W. P. and B. E. Launder (1972). The prediction of laminarization with a two-equation model of turbulence. *International Journal of Heat and Mass Transfer* 15(2), 301-314.

Kim, W. J. and V. C. Patel (1994). Origin and decay of longitudinal vortices in developing flow in a curved rectangular duct (Data bank contribution). *Journal of Fluids Engineering* 116(1), 45-52.

Kreskovsky, J. P., W. R. Briley and H. McDonald (1981). Prediction of laminar and turbulent primary and secondary flows in strongly curved ducts. *NASA Report*, No. CR. 3388.

Lai, H. X., G. L. Xing, S. D. Tu and L. Zhao (2011). A pressure-correction procedure with high-order schemes implemented on unstructured meshes. *International Journal of Numerical Methods for Heat & Fluid Flow* 21(3), 331-352.

Launder, B. E. and D. B. Spalding (1974). The numerical computation of turbulent flows. *Computer Methods in Applied Mechanics and Engineering* 3(2), 269-289.

Launder, B. E. and B. I. Sharma (1974). Application of the energy-dissipation model of turbulence to the calculation of flow near a spinning disc. *Letters in Heat and Mass Transfer* 1(2), 131-137.

Leschziner, M. A. and W. Rodi (1981). Calculation of annular and twin parallel jets using various discretization schemes and turbulence-model variations. *Journal of Fluids Engineering* 103(2), 352-360.

Menter, F. R. (1993). Zonal two equation k–ω models for aerodynamic flows. *AIAA Paper* 93-2906.

Menter, F. R. (1994). Two-equation Eddy-viscosity Turbulence Models for Engineering Applications. *AIAA journal* 32(8), 1598-1605.

Nagano Y. and M. Hishida (1987). Improved Form of the k-ε Model for Wall Turbulent Shear Flows. *Journal of Fluids Engineering* 109(2), 156-160.

Patankar, S. V. (1980). *Numerical Heat Transfer and Fluid Flow*, Taylor and Francis, Philadelphia, London.

Raisee, M., H. Alemi and H. Iacovides (2006). Prediction of developing turbulent flow in 90°□curved ducts using linear and non□linear low□Re k–ε models. *International Journal for Numeethods in Fluids* 51(12), 1379-1405.

Rhie, C. M. (1985). A three-dimensional passage flow analysis method aimed at centrifugal impellers. *Computers and Fluids* 13(4), 443-460.

Shur, M. L., M. K. Strelets and A. K. Travin (2000). Turbulence modeling in rotating and curved channels: Assessing the Spalart-Shur correction. *AIAA journal* 38(5), 784-792.

Spalart, P. R. and M. Shur (1997). On the sensitization of turbulence models to rotation and curvature. *Aerospace Science and Technology* 1(5), 297-302.

Speziale, C. G. and T. Ngo (1988). Numerical solution of turbulent flow past a backward facing step using a nonlinear K-ε model. *International Journal of Engineering Science* 26(10), 1099-1112.

Sudo, K., M. Sumida and H. Hibara (2001). Experimental investigation on turbulent flow in a square-sectioned 90-degree bend. *Experiments in Fluids* 30(3), 246-252.

Suga, K. (2003). Predicting turbulence and heat transfer in 3-D curved ducts by near-wall second moment closures. *International Journal of Heat and Mass Transfer* 46(1), 161-173.

Suzuki, Y. and N. Kasagi (2000). Turbulent air-flow measurement with the aid of 3-D particle tracking velocimetry in a curved square bend. *Flow, Turbulence and Combustion 63(1-4),* 415-442.

Taylor, A, J. H. Whitelaw and M. Yianneskis (1982). Curved ducts with strong secondary motion: velocity measurements of developing laminar and turbulent flow. *Journal of Fluids Engineering* 104(3), 350-359.

Wilcox, D. C. and T. L. Chambers (1977). Streamline curvature effects on turbulent boundary layers. *AIAA Journal* 15(4), 574-580.